First and second harmonic generation of the optical susceptibilities for the non-centro-symmetric orthorhombic $AgCd_2GaS_4$

2008 J. Phys.: Condens. Matter 20 325234

(http://iopscience.iop.org/0953-8984/20/32/325234)

J. Phys.: Condens. Matter **20** (2008) 325234 (6pp) doi:10.1088/0953-8984/20/32/325234

First and second harmonic generation of the optical susceptibilities for the non-centro-symmetric orthorhombic $AgCd_2GaS_4$

Ali H Reshak[1,5], **V V Atuchin**[2], **S Auluck**[3] **and I V Kityk**[4]

[1] Institute of Physical Biology, South Bohemia University, Institute of System Biology and Ecology, Academy of Sciences, Nove Hrady 37333, Czech Republic
[2] Laboratory of Optical Materials and Structures, Institute of Semiconductor Physics, SB RAS, Novosibirsk 90, 630090, Russia
[3] Physics Department, Indian Institute of Technology Kanpur, Kanpur (UP) 208016, India
[4] Silesian University of Technology, Department of Chemistry, Strzody 9, 44-100 Gliwice, Poland

E-mail: maalidph@yahoo.co.uk

Received 3 March 2008, in final form 30 May 2008
Published 18 July 2008
Online at stacks.iop.org/JPhysCM/20/325234

Abstract

We present the results of an *ab initio* theoretical study of the linear and nonlinear optical susceptibilities for the $AgCd_2GaS_4$ using the full potential linearized augmented plane wave (FP-LAPW) method as implemented in the WIEN2K code. We have used the Engel–Vosko exchange–correlation potential which is based on the generalized gradient approximation. Our calculations show that the valence band maximum (VBM) and conduction band minimum (CBM) are located at Γ resulting in a direct energy gap. We present calculations of the frequency-dependent complex dielectric function $\varepsilon(\omega)$. Our calculations show that the edge of the optical absorption for $\varepsilon_2^{xx}(\omega)$ and $\varepsilon_2^{zz}(\omega)$ are located around 2 eV. The linear optical properties show a strong negative uniaxial anisotropy. The optical properties are scissors corrected to match the calculated energy gap with the measured one. The optical properties are analyzed in terms of the calculated electronic structure. The imaginary and real parts of the second-order SHG susceptibility were evaluated. Our calculation shows that $\chi^{(2)}_{333}(\omega)$ is the dominant component which shows the largest *total* Re $\chi^{(2)}_{ijk}(0)$ value 2.0 pm V^{-1}.

(Some figures in this article are in colour only in the electronic version)

1. Introduction

The non-central symmetry of the structure of $AgCd_2GaS_4$ indicates a possibility of using it in nonlinear optics. Moreover, it is photosensitive and develops a considerable luminescence. Taking into consideration the promise of the practical use of this compound, the development of a technology for producing large single crystals is an actual problem. The quaternary sulfide $AgCd_2GaS_4$ has been discovered during an investigation of the quasi-ternary system Ag_2S–CdS–Ga_2S_3 [1, 2]. Recently, single crystal growth of $AgCd_2GaS_4$ has been realized by a solution-melt technique using excess $AgGaS_2$ as a solvent, and single crystal blocks of ∼1 cm^3 scale were selected from the boule [3]. An observation of the optical properties of $AgCd_2GaS_4$ single crystal substrates reveals a energy band gap $E_g = 2.15$ eV and transparency over the spectral range $\lambda = 0.63$–13 μm [3, 4]. In several studies the formation of wide solid solution ranges of $AgCd_2GaS_4$ has been found by substitutions in cation or anion sub-lattices. This crystal may be considered as a parent of a wide family of structure-related 'mixed' crystals where the properties can be tuned through the chemical composition variation [5–9]. The combination of non-centrosymmetric

[5] Author to whom any correspondence should be addressed.

structure and wide transmittance range makes $AgCd_2GaS_4$ a promising material for infra red (IR) nonlinear optical applications. The knowledge of the electronic properties of $AgCd_2GaS_4$, however, is very limited and further investigation is of current interest. The present study is aimed at calculating the linear and nonlinear optical susceptibilities of $AgCd_2GaS_4$ by using the full potential linear augmented plane wave (FP-LAPW) method, which has proven to be one of the most accurate methods [10, 11] for the computation of the electronic structure of solids within density functional theory (DFT). To the best of our knowledge no experimental data and first principles calculation on the linear and nonlinear optical susceptibilities of $AgCd_2GaS_4$ exist in the literature. Therefore a detailed depiction of the electronic properties of $AgCd_2GaS_4$ is timely and would bring us important insights to understanding the origin of the optical properties.

2. Theoretical calculation

$AgCd_2GaS_4$ crystallizes in the non-centrosymmetric orthorhombic space group $Pmn2_1$ (see figure 1).

We have used the experimental lattice constants $a = 8.1395$ Å, $b = 6.9394$ Å, $c = 6.6013$ Å and atomic positions given in [1, 2, 12]. We have performed calculations using the full potential linearized augmented plane wave (FP-LAPW) method as incorporated in the WIEN2K code [13]. This is an implementation of the density functional theory (DFT) [14] with a different possible approximation for the exchange correlation (XC) potentials. The exchange correlation potential was calculated using the generalized gradient approximation (GGA) [22], which is based on exchange–correlation energy optimization to calculate the total energy. We have also used the Engel–Vosko GGA formalism [23], which optimizes the corresponding potential for band structure calculations. It is well known that self-consistent band structure calculations within DFT, both LDA and GGA, usually underestimate the energy gaps [24]. This is mainly due to the fact that they have simple forms that are not sufficiently flexible to accurately reproduce both the exchange correlation energy and its charge derivative. Engel and Vosko considered this shortcoming and constructed a new functional form of GGA [23] which is able to better reproduce the exchange potential at the expense of less agreement in the exchange energy. This approach called EV–GGA, yields better band splitting and some other properties which mainly depend on the accuracy of exchange correlation potential. On the other hand the quantities which depend on an accurate description of the XC potentials, such as the equilibrium volume and bulk modulus, are not in good agreement with experiment [24].

In order to achieve energy eigenvalues convergence, the wavefunctions in the interstitial regions were expanded in plane waves with a cut-off $K_{\max} = 9/R_{MT}$, where R_{MT} denotes the smallest atomic sphere radius and $K_{\max}$ gives the magnitude of the largest K vector in the plane wave expansion. The valence wavefunctions inside the spheres are expanded up to $l_{\max} = 10$ while the charge density was Fourier expanded up to $G_{\max} = 14$ (au)$^{-1}$. The muffin-tin radii were assumed to be 2.35, 2.49, 2.18 and 2.08 au for Ag, Cd, Ga and S respectively.

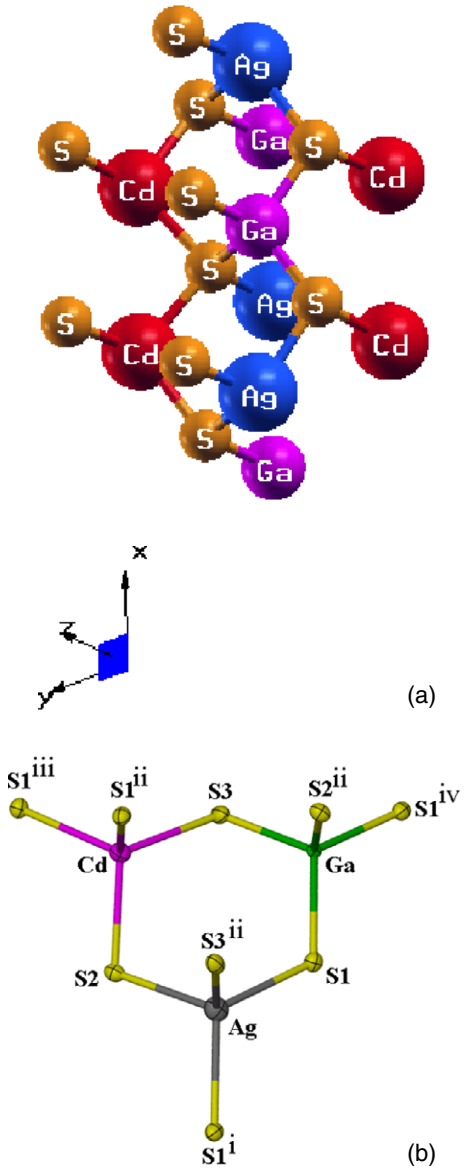

Figure 1. (a) The crystal structure of $AgCd_2GaS_4$. (b) The tetrahedral environment of Ag, Cd and Ga atoms. Displacement ellipsoids are plotted at the 50% probability level. (Symmetry codes: (i) $-x, y, z$; (ii) $1/2 - x, 1 - y, 1/2 + z$; (iii) $x, 1 + y, z$; (iv) $1 - x, y, z$.)

Self-consistency is obtained using 300 **k**-points in the irreducible Brillouin zone (IBZ). The BZ integration was carried out using the tetrahedron method [25, 26]. The linear optical properties are calculated using 500 **k**-points and the nonlinear optical properties are calculated using 1400 **k**-points in IBZ. The self-consistent calculations are considered to have converged if the total energy of the system is stable within 10^{-5} Ryd.

3. Results and discussion

3.1. Linear optical susceptibilities

In general the optical properties of matter can be described by mean of the transverse dielectric function $\varepsilon(\omega)$. There

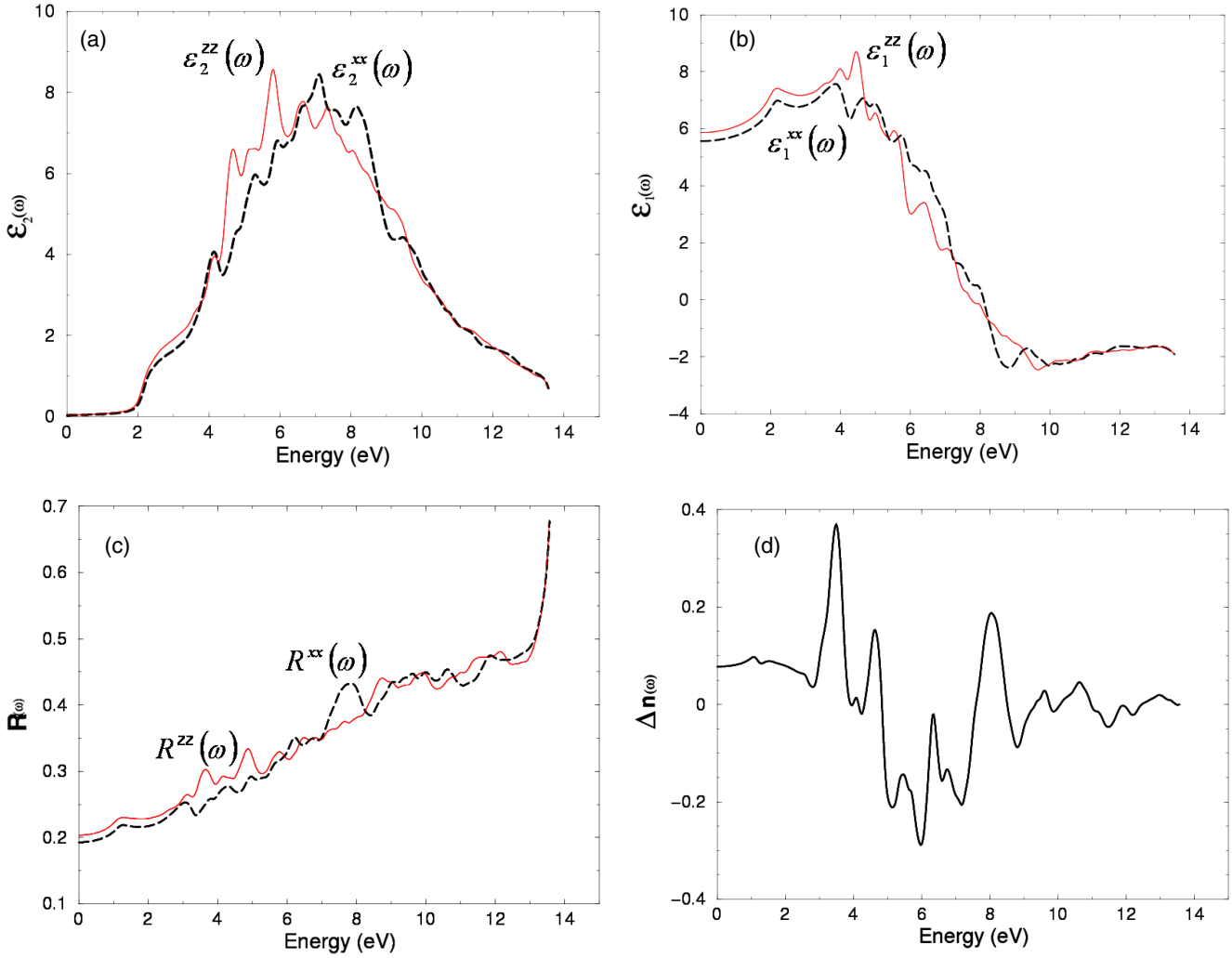

Figure 2. (a) Calculated $\varepsilon_2^{xx}(\omega)$ (dashed curve) and $\varepsilon_2^{zz}(\omega)$ (solid curve) spectra. (b) Calculated $\varepsilon_1^{xx}(\omega)$ (dashed curve) and $\varepsilon_1^{zz}(\omega)$ (solid curve). (c) Calculated $R^{xx}(\omega)$ (dashed curve) and $R^{zz}(\omega)$ (solid curve) spectrum. (d) Calculated $\Delta n(\omega)$ spectrum.

are two contributions to $\varepsilon(\omega)$, namely intraband and interband transitions. The contribution from intraband transitions is important only for metals. The interband transitions can be further split into direct and indirect transitions. Here we neglect the indirect interband transitions which involve scattering of phonon and are expected to give only a small contributions to $\varepsilon(\omega)$ [15]. To calculate the contributions of the direct interband to the imaginary parts of the dielectric function $\varepsilon_2(\omega)$, one must sum up all possible transitions from the occupied to the unoccupied states. Taking the appropriate transition matrix elements into account, we calculated the imaginary part of the dielectric functions $\varepsilon_2(\omega)$ using the expressions given earlier [16, 20].

In the calculations of the optical properties, a dense mesh of uniformly distributed $\boldsymbol{k}$-points is required. Hence, the Brillouin zone integration was performed with 500 $\boldsymbol{k}$-points in the irreducible part of the Brillouin zone. Broadening is taken to be 0.01 eV. Our optical properties are scissor corrected [17, 18] by 0.58 eV. This value is the difference between the calculated (1.57 eV) and measured (2.15 eV) energy gap [4]. This could be traced to the fact that EV–GGA calculations usually underestimate the energy gaps. A very simple way to overcome this drawback is to use the scissor correction, which merely makes the calculated energy gap equal to the experimental gap.

Figure 2(a) displays the variation of the imaginary (absorptive) part of the electronic dielectric function $\varepsilon_2(\omega)$. We note that there is a considerable anisotropy between $\varepsilon_2^{xx}(\omega)$ and $\varepsilon_2^{zz}(\omega)$. Our analysis of the $\varepsilon_2(\omega)$ curve show that the threshold energy (first critical point) of the dielectric function occurs around 2 eV. This corresponds to the Γ_v–Γ_c splitting which gives the threshold for direct optical transitions between the highest valence and the lowest conduction band. As mentioned above, this is around 2.0 eV. We can see from the figure that $\varepsilon_2(\omega)$ shows a sharp rise after 2.0 eV. We define the absorption edge as the energy at which this sharp rise cuts the energy axis. Beyond this point, the curve rises rapidly due to the fact that the number of points contributing towards $\varepsilon_2(\omega)$ increases abruptly.

The peaks in the optical response are caused by the electric–dipole transitions between the valence and conduction bands. In order to identify these structures we need to look at

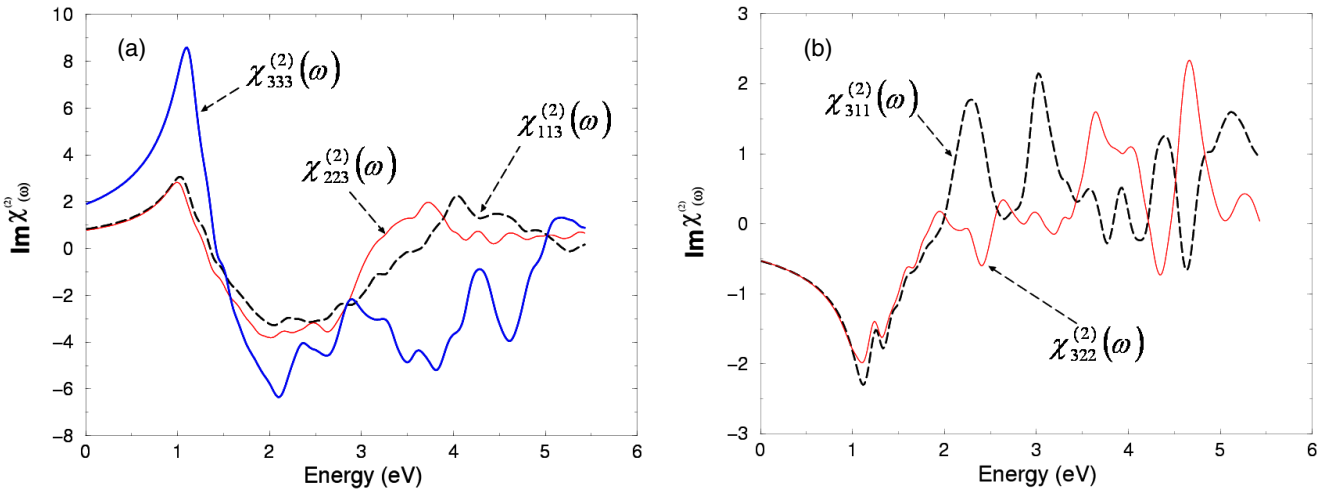

Figure 3. (a) Calculated Im $\chi^{(2)}_{113}(\omega)$, Im $\chi^{(2)}_{223}(\omega)$ and Im $\chi^{(2)}_{333}(\omega)$. (b) Calculated Im $\chi^{(2)}_{311}(\omega)$ and Im $\chi^{(2)}_{322}(\omega)$. All Im $\chi^{(2)}(\omega)$ are multiplied by 10^{-7}, in esu units.

the magnitude of the optical matrix elements. The observed structures would correspond to those transitions which have large optical matrix elements. The critical points are followed by a small hump situated around 4 and 4.5 eV for $\varepsilon_2^{xx}(\omega)$ and $\varepsilon_2^{zz}(\omega)$ respectively. The principle peak in the spectra is situated around 5.5 and 7 eV for $\varepsilon_2^{xx}(\omega)$ and $\varepsilon_2^{zz}(\omega)$ respectively. The main peak in the $\varepsilon_2(\omega)$ spectra are followed by two small humps localized at around 7.5 and 8.5 eV for $\varepsilon_2^{xx}(\omega)$, and 6.5 and 7.3 eV for $\varepsilon_2^{zz}(\omega)$. The main peaks are mainly due to direct transitions between the upper valence band and the second conduction band above the Fermi energy at Γ-edge.

From the imaginary part of the dielectric function $\varepsilon_2^{xx}(\omega)$ and $\varepsilon_2^{zz}(\omega)$ the real part $\varepsilon_1^{xx}(\omega)$ and $\varepsilon_1^{zz}(\omega)$ is calculated by using the Kramers–Kronig relations [19]. The results of our calculated $\varepsilon_1^{xx}(\omega)$ and $\varepsilon_1^{zz}(\omega)$ spectra are shown in figure 2(b). The static dielectric constant $\varepsilon_1(0)$ is given by the low energy limit of $\varepsilon_1(\omega)$. Note that we do not include phonon contributions to the dielectric screening. $\varepsilon_1(0)$ corresponds to the static optical dielectric constant (ε_∞). The calculated value of $\varepsilon_1^{xx}(0)$ is 5.5 and 5.9 for $\varepsilon_1^{zz}(0)$. The uniaxial anisotropy $[\delta\varepsilon = (\varepsilon_0^{\parallel} - \varepsilon_0^{\perp})/\varepsilon_0^{\text{tot}}]$ is −0.037, indicating a strong anisotropy [27] of the dielectric function in $AgCd_2GaS_4$. The calculated reflectivity of $AgCd_2GaS_4$ is shown in figure 2(c). The reflectivity spectra show considerable anisotropy.

3.2. Refraction index and birefringence

Generally a compound which shows considerable anisotropy in the linear optical susceptibilities favors an important quantity in second harmonic generation (SHG) and optical parametric oscillator (OPO) due to better fulfilling of phase matching conditions, determined by birefringence. The birefringence is the difference between the extraordinary and ordinary refractive indices, $\Delta n = n_e - n_0$, where n_e is the index of refraction for an electric field oriented along the **c**-axis and n_0 is the index of refraction for an electric field perpendicular to the **c**-axis [20]. Figure 2(d) shows the spectral behavior of the birefringence $\Delta n(\omega)$ for the $AgCd_2GaS_4$. Birefringence is important only in the non-absorbing region, which is below the energy gap. The $\Delta n(\omega)$ spectral dependence shows strong oscillations around zero in the energy range up to 12.5 eV. We find that the birefringence $\Delta n(0)$ is equal to 0.08. Thus $AgCd_2GaS_4$ is expected to be a phase matchable material.

3.3. Second-order susceptibilities

$AgCd_2GaS_4$ crystallizes in the orthorhombic space group $Pmn2_1$. Based on this symmetry group there are only five independent components of the SHG third rank polar tensor, namely, the 333, 311, 322, 223, and 113 components (1, 2, and 3 refer to the x, y and z axes, respectively) [21]. These are $\chi^{(2)}_{333}(\omega)$, $\chi^{(2)}_{311}(\omega)$, $\chi^{(2)}_{322}(\omega)$, $\chi^{(2)}_{223}(\omega)$ and $\chi^{(2)}_{113}(\omega)$. Here $\chi^{(2)}_{ijk}(\omega)$ is the complex second-order nonlinear optical susceptibility tensor $\chi^{(2)}_{ijk}(-2\omega;\omega;\omega)$ and can be generally written as $\chi^{(2)}_{ijk}(\omega)$. The subscripts i, j, and k are Cartesian indices.

The calculated imaginary part of the second-order SHG susceptibilities $\chi^{(2)}_{333}(\omega)$, $\chi^{(2)}_{311}(\omega)$, $\chi^{(2)}_{322}(\omega)$, $\chi^{(2)}_{223}(\omega)$ and $\chi^{(2)}_{113}(\omega)$ are shown in figure 3. As can be seen the total second-order susceptibility determining SHG is zero below half the band gap. We also show the contributions of ω and 2ω terms. The 2ω term starts contributing at energies $\sim 1/2\ E_g$ and the ω term for energy values above E_g. In the low energy regime ($\leqslant$2.15 eV) the SHG optical spectra is dominated by the 2ω contributions. Beyond 2.15 eV (values of the fundamental energy gaps) the major contribution comes from the ω term.

We have calculated the total complex susceptibility $\chi^{(2)}_{333}(\omega)$, $\chi^{(2)}_{311}(\omega)$, $\chi^{(2)}_{322}(\omega)$, $\chi^{(2)}_{223}(\omega)$ and $\chi^{(2)}_{113}(\omega)$. The real parts are shown in figure 4. The lack of experimental data prevents any conclusive comparison with experiment over a large energy range. We find that $\chi^{(2)}_{333}(\omega)$ is the dominant component which shows the largest total Re $\chi^{(2)}_{ijk}(0)$ value of about 2.0 pm V^{-1}. A definite enhancement in the anisotropy

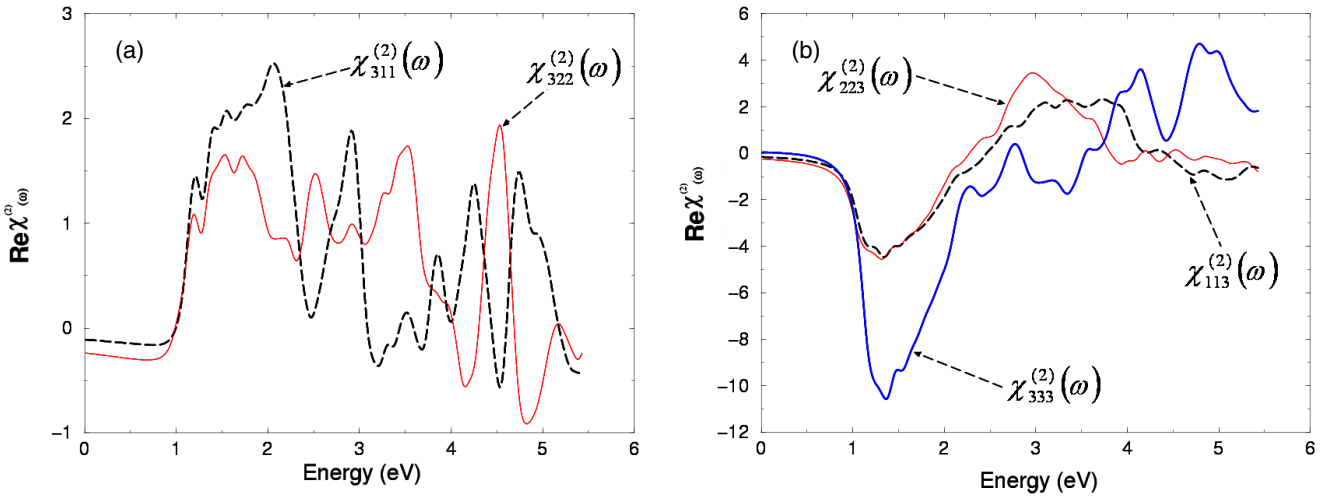

Figure 4. (a) Calculated Re $\chi^{(2)}_{113}(\omega)$, Re $\chi^{(2)}_{223}(\omega)$ and Re $\chi^{(2)}_{333}(\omega)$. (b) Calculated Re $\chi^{(2)}_{311}(\omega)$ and Re $\chi^{(2)}_{322}(\omega)$. All Im $\chi^{(2)}(\omega)$ are multiplied by 10^{-7}, in esu units.

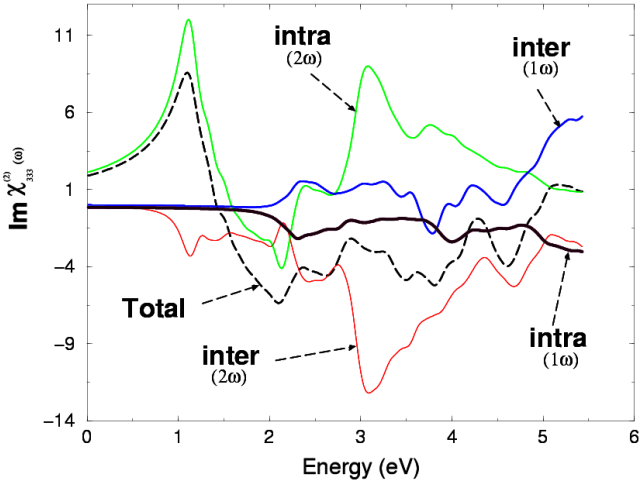

Figure 5. Calculated total Im $\chi^{(2)}_{333}(\omega)$ spectra along with the intra-$(2\omega)/(1\omega)$ and inter-$(2\omega)/(i\omega)$-band contributions. All Im $\chi^{(2)}(\omega)$ are multiplied by 10^{-7}, in esu units.

on going from linear optical properties to the nonlinear optical properties is evident (figures 3 and 4). It is well known that nonlinear optical susceptibilities are more sensitive to small changes in the band structure than the linear optical ones. Hence any anisotropy in the linear optical properties is enhanced more significantly in the nonlinear spectra.

Figure 5 shows the 2ω and ω inter/intraband contributions to the imaginary parts of $\chi^{(2)}_{333}(\omega)$. Note the opposite signs of the two contributions throughout the frequency range. This fact may be useful for molecular engineering of the crystals in the desirable directions.

One could expect that the structures in Im $\chi^{(2)}_{ijk}(\omega)$ could be understood from the features of $\varepsilon_2(\omega)$. Unlike the linear optical spectra, the features in the SHG susceptibility are very difficult to identify from the band structure because of the superposition of 2ω and ω terms. But we make use of the linear optical spectra to identify the different resonances leading to various features in the SHG spectra. The first spectral band in Im $\chi^{(2)}_{333}(\omega)$ between 0.0 and 3.0 eV is mainly from the 2ω resonance and arises from the first structure in $\varepsilon_2(\omega)$. The second structure between 3.0 and 4.0 eV is associated with interference between the ω resonance and 2ω resonance and it is associated with high energy structure in $\varepsilon_2(\omega)$. The last structure from 4.0 to 5.5 eV is mainly due to the ω resonance and is associated with the tail in $\varepsilon_2(\omega)$. It is interesting to add that such features are present in defect chalcopyrite crystal structures [28].

4. Conclusions

We have performed first principle calculations of the linear and nonlinear optical susceptibilities for the $AgCd_2GaS_4$ using the FP-LAPW method. Our calculations show that the edges of optical absorption for $\varepsilon_2^{xx}(\omega)$ and $\varepsilon_2^{zz}(\omega)$ are located around 2 eV. The imaginary and real parts of the second-order SHG susceptibility were evaluated. We note that any anisotropy in the linear optical susceptibilities will significantly enhance the nonlinear optical susceptibilities. The 2ω and 1ω inter/intraband contributions to the imaginary parts of $\chi^{(2)}_{333}(\omega)$ show opposite signs. This fact may be used in future for molecular engineering of the crystals in desirable directions. Our calculation shows that $\chi^{(2)}_{333}(\omega)$ is the dominant component showing the largest *total* Re $\chi^{(2)}_{ijk}(0)$.

Acknowledgments

This work was supported from the institutional research concept of the Institute of Physical Biology, UFB (No. MSM6007665808), and the Institute of System Biology and Ecology, ASCR (No. AVOZ60870520).

References

[1] Chykhrij S I, Parasyuk O V and Halka V O 2000 Crystal structure of the new quaternary phase $AgCd_2GaS_4$ and phase

diagram of the quasi-binary system $AgGaS_4$–CdS *J. Alloys Compounds* **312** 189–95
[2] Olekseyuk I D, Parasyuk O V, Halka V O, Piskach L V, Pankevych V Z and Romanyuk Y E 2001 Phase equilibria in the quasi-ternary system Ag_2S–CdS–Ga_2S_3 *J. Alloys Compounds* **325** 167–79
[3] Olekseyuk I D, Parasyuk O V, Yurchenko O M, Pankevich V Z, Zaremba V I, Valiente R and Romanyuk Y E 2005 Single-crystal growth and properties of $AgCd_2GaS_4$ *J. Cryst. Growth* **279** 140–5
[4] Atuchin V V, Pankevich V Z, Parasyuk O V, Pervukhina N V, Pokrovsky L D, Remesnik V G, Uvarov V N and Pekhnyo V I 2006 *J. Cryst. Growth* **292** 494–9
[5] Olekseyuk I D, Husak O A, Gulay L D and Parasyuk O V 2004 The $AgGaS_2 + 2CdSe \Leftrightarrow AgGaSe_2 + 2CdS$ system *J. Alloys Compounds* **367** 25–35
[6] Davydyuk G E, Olekseyuk I D, Parasyuk O V, Voronyuk S V, Husak O A and Pekhnyo V I 2005 Solid solutions of the $AgCd_2GaS_4$–$AgCd_2GaSe_4$ system, their electric and photoelectric properties *Ukr. J. Phys.* **50** 679–84
[7] Olekseyuk I D, Parasyuk O V, Husak O A, Piskach L V, Volkov S V and Pekhnyo V I 2005 X-ray powder diffraction study of semiconducting alloys $Ag_{1-x}Cu_xCd_2GaS_4$ and $AgCd_2Ga_{1-x}In_xS_4$ *J. Alloys Compounds* **402** 186–93
[8] Parasyuk O V, Olekseyuk I D, Dzham O A and Pekhnyo V I 2006 Synthesis and x-ray powder diffraction studies of semiconducting alloys in the system $AgCd_{2-x}Zn_xGaS_4$ *Cryst. Res. Technol.* **41** 32–6
[9] Davydyuk G Ye, Sachanyuk V P, Voronyuk S V, Olekseyuk I D, Romanyuk Y E and Parasyuk O V 2006 X-ray diffraction study of the $AgCd_{2-x}Mn_xGaS_4$ semiconductor alloys and their electrical, optical, and photoelectrical properties *Physica* B **373** 355–9
[10] Gao S 2003 *Comput. Phys. Commun.* **153** 190–8
[11] Schwarz K 2003 *J. Solid State Chem.* **176** 319–28
[12] Pervukhina N V, Atuchin V V and Parasyuk O V 2005 Redermination of the quaternary phase silver dicadmium tetrasulfide, $AgCd_2GaS_4$ *Acta Crystallogr.* E **61** i91–i93
[13] Blaha P, Schwarz K, Madsen G K H, Kvasnicka D and Luitz J 2001 *WIEN2K, an Augmented Plane Wave + Local Orbitals Program for Calculating Crystal Properties* ed K Schwarz, Techn. Universitat, Wien, Austria ISBN 3-9501031-1-2
[14] Hohenberg P and Kohn W 1964 *Phys. Rev.* B **136** 864
[15] Smith N V 1862 *Phys. Rev.* B **3** 1971
[16] Hufner S, Claessen R, Reinert F, Straub Th, Strocov V N and Steiner P 1999 *J. Electron Spectrosc. Relat. Phenom.* **100** 191
Ahuja R, Auluck S, Johansson B and Khan M A 1994 *Phys. Rev.* B **50** 2128
[17] Levine B F 1973 *Phys. Rev.* B **7** 2600 and references therein
[18] Nastos F, Olejnik B, Schwarz K and Sipe J E 2005 *Phys. Rev.* B **72** 045223
[19] Tributsch H 1977 *Z. Naturf.* A **32A** 972
[20] Wooten F 1972 *Optical Properties of Soilds* (New York: Academic)
[21] Boyd W 1992 *Nonlinear Optics* (Boston, MA: Academic)
[22] Perdew J P, Burke S and Ernzerhof M 1996 *Phys. Rev. Lett.* **77** 3865
[23] Engel E and Vosko S H 1993 *Phys. Rev.* B **47** 13164
[24] Dufek P, Blaha P and Schwarz K 1994 *Phys. Rev.* B **50** 7279
[25] Jepsen O and Andersen O K 1971 *Solid State Commun.* **9** 1763
Lehmann G and Taut M 1972 *Phys. Status Solidi* B **54** 496
[26] Wilson J A and Yoffe A D 1969 *Adv. Phys.* **18** 193
[27] Reshak A H 2005 *PhD Thesis* Indian Institute of Technology-Rookee, India
[28] Dovgii Ya O, Kityk I V and Caryk amd A V 1991 *Ukr. Phys. J.* V **36** 52